Phonon-Mediated Nonclassical Interference in Diamond

Duncan G. England,[1] Kent A. G. Fisher,[2] Jean-Philippe W. MacLean,[2] Philip J. Bustard,[1] Khabat Heshami,[1] Kevin J. Resch,[2] and Benjamin J. Sussman[1,3,*]

[1]National Research Council of Canada, 100 Sussex Drive, Ottawa, Ontario K1A 0R6, Canada
[2]Institute for Quantum Computing and Department of Physics and Astronomy, University of Waterloo, 200 University Avenue West, Waterloo, Ontario N2L 3G1, Canada
[3]Department of Physics, University of Ottawa, Ottawa, Ontario K1N 6N5, Canada

(Received 4 May 2016; published 11 August 2016)

Quantum interference of single photons is a fundamental aspect of many photonic quantum processing and communication protocols. Interference requires that the multiple pathways through an interferometer be temporally indistinguishable to within the coherence time of the photon. In this Letter, we use a diamond quantum memory to demonstrate interference between quantum pathways, initially temporally separated by many multiples of the optical coherence time. The quantum memory can be viewed as a light-matter beam splitter, mapping a THz-bandwidth single photon to a variable superposition of the output optical mode and stored phononic mode. Because the memory acts both as a beam splitter and as a buffer, the relevant coherence time for interference is not that of the photon, but rather that of the memory. We use this mechanism to demonstrate nonclassical single-photon and two-photon interference between quantum pathways initially separated by several picoseconds, even though the duration of the photons themselves is just ~250 fs.

DOI: 10.1103/PhysRevLett.117.073603

Single photons are an attractive choice of qubit but the interaction between two single photons is weak, making the implementation of deterministic two-photon gates between two photons challenging [1]. One option is to exploit the interference of single photons at optical beam splitters, combined with feed-forward techniques, to build probabilistic logic gates [2]. However, the probabilistic nature of these gates is a barrier to the scalability of linear-optical quantum processors and, thus far, demonstrations have been limited to small numbers of qubits [3]. Quantum memories—devices that can store a quantum state of light and release it on demand—have been proposed as a solution to the scalability problem [4,5]. By acting as a buffer for single photons, a quantum memory allows storage during feed-forward operations [6,7], and synchronization of multiple probabilistic events [8].

Beyond acting as a buffer, it has been shown that a quantum memory can behave as a light-matter beam splitter that partitions an excitation between the light mode, a photon, and the matter mode, a material excitation [see Figs. 1(a) and 1(b)]. In the classical regime, this functionality has previously been exploited to investigate interference between atomic spin coherences and an optical field [9], and to develop new capabilities such as reconfigurable optical components [10] and a mirrorless optical resonator [11]. At the quantum level, interference in a quantum memory has been used as a qubit analyzer to demonstrate entanglement between a single photon and a hybrid light-matter qubit [12]. Furthermore, it has been proposed that quantum memories with beam-splitter functionality could be used for continuous-variable quantum computing in the time domain [13], or to perform unitary transforms and linear logic gates [14]. In these proposals, the quantum memory both stores the single photons and performs linear operations upon them, and therefore offers a promising route toward scalable linear-optical quantum computing.

Here we use a diamond quantum memory [15,16] to investigate quantum interference phenomena with THz-bandwidth single photons. The memory mediates nonclassical single- and multiphoton interference effects between quantum pathways that, in the absence of the memory, would otherwise be temporally distinguishable. In

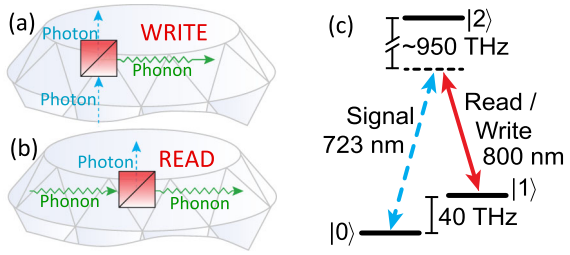

FIG. 1. (a) The write interaction of the diamond quantum memory is analogous to a beam splitter partitioning an input photon between the photon and phonon modes. (b) Similarly, the read interaction also behaves as a beam splitter. (c) Energy level diagram of the diamond memory. The diamond crystal is initially in the ground state $|0\rangle$. The signal photon (723 nm) and the read-write pulses (800 nm) are in two-photon resonance with the optical phonon mode $|1\rangle$, but far detuned from the conduction band $|2\rangle$.

the first experiment, a single photon is partitioned between two time-bin modes. The first time-bin mode ($B1$) is written, with efficiency R_1, into the memory; when a read pulse retrieves this excitation while simultaneously writing time-bin mode $B2$ into the memory (with efficiency R_2) interference is detected in the output optical mode. In the second experiment, a weak coherent state is written into the memory in time bin $B1$; when a read pulse retrieves this excitation while simultaneously writing a single photon into the memory, nonclassical photon bunching is observed in the output optical mode.

The memory dynamics can be modeled as a beam-splitter interaction, where the single-photon mode with creation operator $a^\dagger$ is partially mapped to a phonon mode with creation operator $b^\dagger$, thereby creating a superposition,

$$a^\dagger e^{i\omega_a t} \rightarrow i\sqrt{R_1} b^\dagger e^{i\omega_b t} + \sqrt{1-R_1} a^\dagger e^{i\omega_a t}. \quad (1)$$

Here the write efficiency of the memory R_1 is analogous to the reflectivity of the beam splitter [17], and ω_a, ω_b are the oscillation frequencies of the photon and phonon, respectively. Similarly, the retrieval of a photon from the memory can be written as

$$b^\dagger e^{i\omega_b t} \rightarrow i\sqrt{R_2} a^\dagger e^{i\omega_a t} + \sqrt{1-R_2} b^\dagger e^{i\omega_b t}, \quad (2)$$

where R_2 is the read efficiency of the memory. Between the write and read interactions, the photon is stored in the memory for a storage time τ; during this time the phase of the phonon evolves, and its amplitude decays, resulting in loss from the memory. We model the loss as a beam splitter with time-dependent transmission $T(\tau)$,

$$b^\dagger e^{i\omega_b t} \rightarrow \sqrt{T(\tau)} b^\dagger e^{i\omega_b (t+\tau)} + \sqrt{1-T(\tau)} d^\dagger, \quad (3)$$

where $T(\tau) = e^{-\tau/\tau_0}$. The operator $d^\dagger$ encompasses any form of loss during storage, the predominant mechanism being the decay of an optical phonon into a pair of acoustic phonons via the Klemens channel [18], with lifetime $\tau_0 = 3.5$ ps [19].

Experiment.—The diamond quantum memory is described by the Λ-level system shown in Fig. 1(c) where the initial state $|0\rangle$ corresponds to the ground state of the crystal lattice and the storage state $|1\rangle$ is the optical phonon band. A signal photon (wavelength 723 nm) is stored in, and retrieved from, the optical phonon modes by the write and read pulses (wavelength 800 nm). The signal and read-write pulses are in two-photon Raman resonance with the optical phonon frequency (40 THz) and are far detuned from the conduction band, $|2\rangle$. The diamond, which is 2.3 mm thick, was grown by chemical vapor deposition and is cut on the $\langle 100 \rangle$ face. In this configuration, the Raman interaction couples fields of orthogonal polarization such that a vertically polarized write pulse is used to store horizontally polarized light and a horizontally polarized read pulse is used to retrieve a vertically polarized output [15].

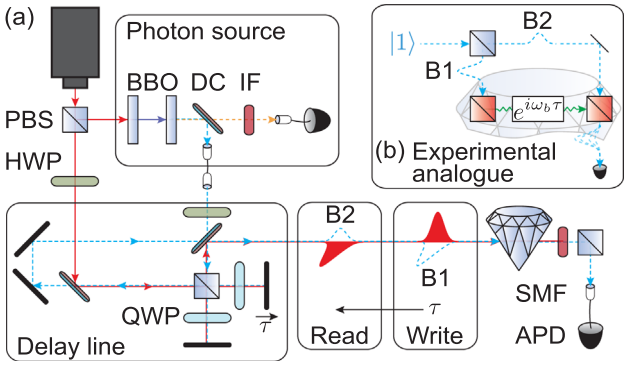

FIG. 2. (a) Experimental diagram for single-photon interference. A single photon from the SPDC photon source (dashed blue) is split into two time bins, in the first ($B1$) the photon is horizontally polarized, and in the second ($B2$) vertically polarized. Each time bin is overlapped with orthogonally polarized read and write pulses (solid red) resulting in interference in the second time bin. BBO: β-barium borate; HWP/QWP: half-/quarter-wave plate; PBS: polarizing beam splitter; DC: dichroic mirror; IF: interference filter; SMF: single-mode fiber. (b) Conceptual setup. The single photon is partitioned into two time bins by an optical beam splitter (blue). Each time bin then impinges upon a memory beam splitter (red) separated by a time delay τ.

The master laser for the experiment is a mode-locked titanium:sapphire laser oscillator with a central wavelength of 800 nm, pulse duration of 190 fs, and a pulse repetition rate of 80 MHz. The read and write pulses, each of energy ~6 nJ, are derived from the oscillator. Single photons are produced by a nondegenerate spontaneous parametric down-conversion (SPDC) photon pair source where the detection of a herald photon (895 nm) implies the presence of the signal photon (723 nm) and triggers the experiment (see Ref. [16] for details). At the output of the memory, photons are measured on an avalanche photodiode (APD), and timing correlations with the herald are measured using coincidence counting logic.

Single-photon interference.—To demonstrate single-photon interference in this system, the photon from the SPDC source is partitioned into two orthogonally polarized time bins $B1$ and $B2$ by a polarization-dependent optical delay line (see Fig. 2). The 800 nm pulse is also sent through the delay line to generate the read and write pulses. The signal photon is horizontally polarized at $B1$ and vertically polarized at $B2$; in each time bin the write ($B1$) or read ($B2$) pulse is orthogonally polarized to the signal to enable the necessary Raman coupling. The delay τ between the two time bins is coarsely tuned by a motorized delay stage, and fine control is achieved using a piezoelectric actuator [20]. After the diamond, the photons are spectrally isolated from the control pulses by interference filters, and a polarizer is used to select the horizontally (vertically) polarized photons in $B1$ ($B2$).

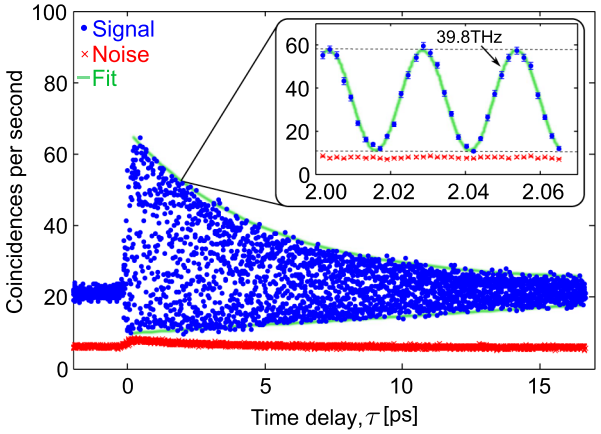

FIG. 3. Signal-herald coincidences (blue dots) and memory noise (red crosses) as a function of time delay τ between $B1$ and $B2$, with an exponential fit to the envelope (green line). Inset: High-resolution scan around delay $\tau = 2$ ps exhibiting interference fringes of frequency 39.8 ± 0.9 THz, extracted via a sinusoidal fit.

We begin with a horizontally polarized signal photon such that all of the photons arrive in $B1$. When we apply the write pulse at $B1$, a dip of $11.0 \pm 0.8\%$ in the signal-herald coincidence rate is observed due to Raman absorption of the signal photons. The reflectivity of the first memory beam splitter is therefore $R_1 = 11\%$. The width of this absorption dip, measured by scanning the arrival time of the write laser, is 326 fs [16]. Deconvolving the write pulse duration (190 fs) returns a photon duration of 264 fs. We then set the delay τ between the two time bins to be 1 ps and apply the read pulse in $B2$ to retrieve vertically polarized photons from the memory with overall memory efficiency of $\eta = 1.20 \pm 0.04\%$. The reflectivity of the second beam splitter is then $R_2 = \eta/R_1 = 11 \pm 1\%$.

Next, we rotate the polarization of the input signal photon such that a small fraction of the photons arrive at the memory in time bin $B2$. There are two ways in which a photon can be detected in time bin $B2$ at the memory output: either the photon originated in $B2$ and was simply transmitted by the memory, or the photon originated in $B1$, was stored, and then recalled into $B2$ by the read pulse. These two pathways constructively and destructively interfere, resulting in a detection probability that oscillates as a function of the time delay τ between the two time bins, as can be seen in Fig. 3. By adjusting the input polarization we balance the amplitudes of the two pathways resulting in maximum interference visibility.

The functional form of the interference pattern in Fig. 3 can be derived by considering the action of transformations (1)–(3) on initial photon input state $(p_1 a^\dagger_{B1} + p_2 a^\dagger_{B2})|0\rangle$, where p_1 and p_2 are the input population amplitudes in time bin $B1$ and $B2$, respectively. We apply transformation (1), (3), and then (2) to $a^\dagger_{B1}$, and transformation (1) to $a^\dagger_{B2}$ returning

$$a^\dagger_{B1} e^{i\omega_a t} \rightarrow -R a^\dagger_{B2} e^{i\omega_b \tau} e^{i\omega_a t} e^{-\tau/2\tau_0} + \sqrt{1-R}\, a^\dagger_{B1} e^{i\omega_a t},$$
$$a^\dagger_{B2} e^{i\omega_a t} \rightarrow i\sqrt{R} b^\dagger e^{i\omega_b t} e^{-t/2\tau_0} + \sqrt{1-R}\, a^\dagger_{B2} e^{i\omega_a t}. \quad (4)$$

Here, $R = R_1 = R_2 = 11\%$. The expected photon number in $B2$ is therefore

$$\begin{aligned}\langle a^\dagger_{B2} a_{B2}\rangle &= |-p_1 R e^{i\omega_b \tau} e^{-\tau/2\tau_0} + p_2\sqrt{1-R}|^2, \\ &= R^2 p_1^2 e^{-\tau/\tau_0} + (1-R)p_2^2 \\ &\quad - 2R\sqrt{1-R}\, p_1 p_2 e^{-\tau/2\tau_0}\cos(\omega_b \tau). \end{aligned} \quad (5)$$

This shows the two key features of the phonon-mediated interference. First, the interference visibility decreases with storage time due to the decay of the optical phonon, as can be seen in Fig. 3. Secondly, the interference fringes oscillate at the phonon frequency $\omega_b/2\pi = 40$ THz, rather than the optical frequency of the photon ($\omega_a/2\pi = 415$ THz) as can be seen in the inset of Fig. 3.

The memory output includes noise photons (shown in red crosses in Fig. 3), which are present even when no photon is stored. The noise is generated by a mixture of thermal anti-Stokes scattering and four-wave mixing [16,21]. Because the noise processes are spontaneous, they do not contribute to the interference and simply degrade the visibility. The visibility is extracted by fitting the envelope of the interference pattern in Fig. 3 (green line) and reaches a peak of 73%. It is important to note that interference persists for over 60 times the duration of the photon (264 fs). The longevity of the interference pattern demonstrates that the quantum memory can be used to mediate interference between two temporally distinct quantum pathways traversed by a single photon. In the next experiment, we show that this technique can be extended to multiphoton quantum interference effects.

Two-photon interference.—The archetypal multiphoton interference effect is Hong-Ou-Mandel (HOM) interference, the signature of which is photon bunching, where identical single photons, incident upon the two input ports of a beam splitter, emerge together from the same output port due to quantum interference. HOM interference can be observed between two single photons, or between a photon and a weak coherent state [22], and is often detected by measuring a "dip" in coincident detections between the two output modes [23].

To investigate HOM interference in the memory, we use two light sources: the SPDC source and an optical parametric oscillator (OPO) that is synchronously pumped by the master laser oscillator. The OPO output can be modeled by a coherent state [24], $|\alpha_l\rangle$, which is attenuated such that the mean photon number at the diamond is $|\alpha_l|^2 \approx 2.5$ per pulse. The amplitude of the coherent state is chosen such that multiphoton components in the memory output ($|\alpha_{\text{out}}|^2 \approx 0.025$) are negligible while maintaining sufficient count rates to measure two-photon interference. The

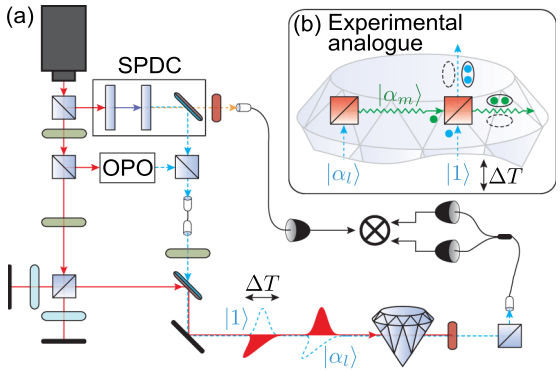

FIG. 4. (a) Experimental setup figure for two-photon interference. The master laser pumps two independent sources of photons. The SPDC source produces single photons $|1\rangle$, and an optical parametric oscillator (OPO) produces a coherent state of amplitude $|\alpha_l|^2 = 2.5$ photons per pulse. The coherent state is stored in the memory by the write pulse creating a phonon excitation. After a delay of $\tau = 1$ ps, the single photon and the read pulse arrive at the memory and the photon interferes with the phonon excitation resulting in HOM-type bunching. The two-photon component of the optical output field is detected using a 50:50 fiber beam splitter and two APDs. (b) Conceptual setup. A coherent state of light $|\alpha_l\rangle$ is reflected at the first memory beam splitter creating a phonon excitation $|\alpha_m\rangle$. The phonon excitation combines with a single photon on the second memory beam splitter resulting in bunching.

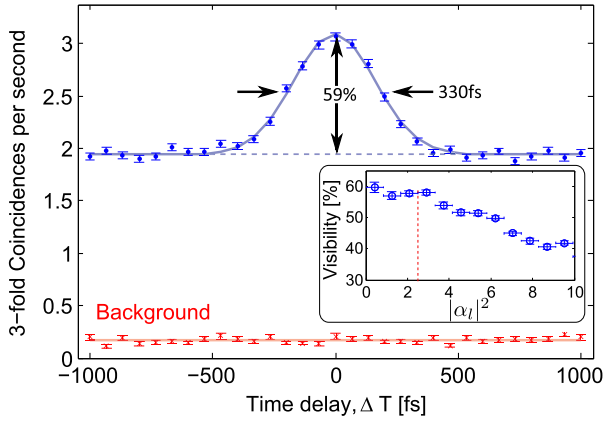

FIG. 5. Threefold coincident detections of a herald photon and two photons in the output of the quantum memory as a function of delay ΔT between the single photon and the memory read pulse (blue dots). A peak at zero delay is evidence of Hong-Ou-Mandel-type bunching. The background rate (red crosses) is obtained when the pulse order is reversed (see the text). Inset: HOM visibility as a function of coherent state amplitude. The red dashed line indicates the value chosen for the main plot ($|\alpha_l|^2 \approx 2.5$)

coherent state and single photon are combined on a polarizing beam splitter (PBS) and coupled into the same single-mode fiber before being sent to the memory (see Fig. 4). The horizontally polarized coherent state arrives first at the memory and is stored with efficiency $R_1 = 10\%$. The resulting phonon excitation $|\alpha_m\rangle = \sqrt{R_1}|\alpha_l\rangle$ contains, on average, $|\alpha_m|^2 \approx 0.25$ phonons per laser pulse. The vertically polarized single photon arrives at the memory 1 ps after the coherent state, along with the read pulse. The output from the second time bin is selected by a polarizer, and coupled into a fiber for photon counting.

In the ideal case, bunching results in either two photons exiting the memory or two phonons remaining in storage. Because it is difficult to measure the phonon port of the memory beam splitter, we cannot measure a conventional HOM dip. Instead, we measure a peak in two-photon detection in the optical output of the memory as our accessible signature of HOM interference; a similar approach has been employed in optical HOM interference [25,26]. In the absence of photon-number-resolving detectors [27], we measure two-photon events by splitting the optical mode on a 50:50 fiber beam splitter and detecting on two separate APDs, as shown in Fig. 4. Our metric is therefore the rate of threefold coincident detections of a herald photon and a photon in each arm of the fiber beam splitter. Figure 5 shows threefold detection rates as a function of delay between the single photon and the read pulse, ΔT; a peak at zero delay demonstrates HOM interference between single photons and the weak coherent state, mediated by the quantum memory. The width of the peak is 330 ± 10 fs, in good agreement with the cross-correlation between the single photon and the read-write pulses as measured by photon absorption (326 fs [16]). The background threefold rate (red crosses in Fig. 5) is measured by reversing the pulse order such that the single photons arrive at the memory 5 ps before the coherent state. In this case, threefold counts result from accidental coincidences between single photons and memory noise, and no HOM interference is visible.

The raw visibility of the HOM peak is $59 \pm 2\%$, and the background-subtracted visibility is $65 \pm 3\%$. The HOM visibility as a function of the coherent state amplitude $|\alpha_l|^2$ is plotted in the inset of Fig. 5. The visibility does not exceed 60%, even as $|\alpha_l|^2$ approaches 0 where the two-photon contribution becomes negligible; hence, multiphoton components in the weak coherent state are not the limiting factor on our HOM visibility for $|\alpha_l|^2 \leq 2.5$. Instead, the visibility is limited by spectral and temporal mismatch between $|1\rangle$ and $|\alpha_l\rangle$.

In conclusion, we have demonstrated single-photon and two-photon nonclassical interference effects via a diamond quantum memory. The quantum memory acts as a beam splitter and also as a buffer, removing the requirement to construct a separate delay line to overlap the two photons. This technique is not unique to diamond and could be applied to other quantum memories with longer storage times [28,29]. In this case two photons, with variable delays of several hundred ns, could be interfered at the memory beam splitter, a functionality that would be extremely challenging with linear optics. In the future, quantum memories of this type could be used to build rapidly

reconfigurable optical components for linear-optical quantum processing applications [13,14,30]. As these components scale to large numbers of operations, failures due to imperfect interference visibility accumulate; minimizing memory noise is therefore a key challenge for future scalability.

This work was supported by the Natural Sciences and Engineering Research Council of Canada, Canada Research Chairs, Canada Foundation for Innovation, Industry Canada, Ontario Centres of Excellence, and Ontario Ministry of Research and Innovation Early Researcher Award. The authors are grateful to Matthew Markham and Alastair Stacey of Element Six Ltd. for manufacturing the diamond sample and to Doug Moffatt and John Donohue for software assistance. They also acknowledge fruitful discussions with Michael Spanner, Rune Lausten, Paul Hockett, and Josh Nunn, and technical support from Denis Guay.

*ben.sussman@nrc.ca

[1] D. E. Chang, V. Vuletić, and M. D. Lukin, Nat. Photonics **8**, 685 (2014).
[2] E. Knill, R. Laflamme, and G. J. Milburn, Nature (London) **409**, 46 (2001).
[3] J. L. O'Brien, G. J. Pryde, A. G. White, T. C. Ralph, and D. Branning, Nature (London) **426**, 264 (2003).
[4] F. Bussières, N. Sangouard, M. Afzelius, H. de Riedmatten, C. Simon, and W. Tittel, J. Mod. Opt. **60**, 1519 (2013).
[5] K. Heshami, D. G. England, P. C. Humphreys, P. J. Bustard, V. M. Acosta, J. Nunn, and B. J. Sussman, J. Mod. Opt. **63**, S42 (2016).
[6] T. B. Pittman, B. C. Jacobs, and J. D. Franson, Phys. Rev. A **66**, 042303 (2002).
[7] Z.-S. Yuan, Y.-A. Chen, S. Chen, B. Zhao, M. Koch, T. Strassel, Y. Zhao, G.-J. Zhu, J. Schmiedmayer, and J.-W. Pan, Phys. Rev. Lett. **98**, 180503 (2007).
[8] J. Nunn, N. K. Langford, W. S. Kolthammer, T. F. M. Champion, M. R. Sprague, P. S. Michelberger, X.-M. Jin, D. G. England, and I. A. Walmsley, Phys. Rev. Lett. **110**, 133601 (2013).
[9] G. Campbell, M. Hosseini, B. M. Sparkes, P. K. Lam, and B. C. Buchler, New J. Phys. **14**, 033022 (2012).
[10] K. F. Reim, J. Nunn, X.-M. Jin, P. S. Michelberger, T. F. M. Champion, D. G. England, K. C. Lee, W. S. Kolthammer, N. K. Langford, and I. A. Walmsley, Phys. Rev. Lett. **108**, 263602 (2012).
[11] O. Pinel, J. L. Everett, M. Hosseini, G. T. Campbell, B. C. Buchler, and P. K. Lam, Sci. Rep. **5**, 17633 (2015).
[12] C. Clausen, I. Usmani, F. Bussieres, N. Sangouard, M. Afzelius, H. de Riedmatten, and N. Gisin, Nature (London) **469**, 508 (2011).
[13] P. C. Humphreys, W. S. Kolthammer, J. Nunn, M. Barbieri, A. Datta, and I. A. Walmsley, Phys. Rev. Lett. **113**, 130502 (2014).
[14] G. T. Campbell, O. Pinel, M. Hosseini, T. C. Ralph, B. C. Buchler, and P. K. Lam, Phys. Rev. Lett. **113**, 063601 (2014).
[15] D. G. England, P. J. Bustard, J. Nunn, R. Lausten, and B. J. Sussman, Phys. Rev. Lett. **111**, 243601 (2013).
[16] D. G. England, K. A. G. Fisher, Jean-Philippe W. MacLean, P. J. Bustard, R. Lausten, K. J. Resch, and B. J. Sussman, Phys. Rev. Lett. **114**, 053602 (2015).
[17] Z. Ou, C. Hong, and L. Mandel, Opt. Commun. **63**, 118 (1987).
[18] P. G. Klemens, Phys. Rev. **148**, 845 (1966).
[19] K. Lee, B. Sussman, M. Sprague, P. Michelberger, K. Reim, J. Nunn, N. Langford, P. Bustard, D. Jaksch, and I. Walmsley, Nat. Photonics **6**, 41 (2012).
[20] The displacement of the piezoelectric actuator as a function of applied voltage was calibrated using optical interferometry.
[21] N. Lauk, C. O'Brien, and M. Fleischhauer, Phys. Rev. A **88**, 013823 (2013).
[22] J. G. Rarity, P. R. Tapster, and R. Loudon, J. Opt. B **7**, S171 (2005).
[23] C. K. Hong, Z. Y. Ou, and L. Mandel, Phys. Rev. Lett. **59**, 2044 (1987).
[24] R. J. Glauber, Phys. Rev. **131**, 2766 (1963).
[25] J. G. Rarity and P. R. Tapster, J. Opt. Soc. Am. B **6**, 1221 (1989).
[26] K. Mattle, H. Weinfurter, P. G. Kwiat, and A. Zeilinger, Phys. Rev. Lett. **76**, 4656 (1996).
[27] A. J. Miller, S. W. Nam, J. M. Martinis, and A. V. Sergienko, Appl. Phys. Lett. **83**, 791 (2003).
[28] K. Reim, J. Nunn, V. Lorenz, B. Sussman, K. Lee, N. Langford, D. Jaksch, and I. Walmsley, Nat. Photonics **4**, 218 (2010).
[29] P. J. Bustard, R. Lausten, D. G. England, and B. J. Sussman, Phys. Rev. Lett. **111**, 083901 (2013).
[30] K. R. Motes, A. Gilchrist, J. P. Dowling, and P. P. Rohde, Phys. Rev. Lett. **113**, 120501 (2014).